

# Multi-locational Majorana Zero Modes

Yutaro Nagae,<sup>1,\*</sup> Andreas P. Schnyder,<sup>2</sup> Yukio Tanaka,<sup>1</sup> Yasuhiro Asano,<sup>3</sup> and Satoshi Ikegaya<sup>1,4,\*</sup>

<sup>1</sup>*Department of Applied Physics, Nagoya University, Nagoya 464-8603, Japan*

<sup>2</sup>*Max-Planck-Institut für Festkörperforschung, Heisenbergstrasse 1, D-70569 Stuttgart, Germany*

<sup>3</sup>*Department of Applied Physics, Hokkaido University, Sapporo 060-8628, Japan*

<sup>4</sup>*Institute for Advanced Research, Nagoya University, Nagoya 464-8601, Japan*

(Dated: June 26, 2023)

Beyond the framework of the bulk-boundary correspondence, we predict the emergence of a Majorana zero mode that is not bounded at one end of a topological superconductor as conventional, but splits into multiple parts which are located at the distant ends of different topological superconductors. We refer to this remarkable zero mode, which exhibits simultaneously the Majorana property and extreme nonlocality, as a multi-locational Majorana zero mode. Specifically, we discuss multi-locational Majorana zero modes in a three-terminal Josephson junction consisting of topological superconductors, which forms an elemental qubit of fault-tolerant topological quantum computers. The multi-locational Majorana zero modes give rise to highly entangled and anomalously long-ranged nonlocal resonant transport phenomena, which can be utilized to verify conclusively the realization of a fully functional topological three-terminal Josephson junction.

*Introduction.*—Majorana zero modes (MZMs) of topological superconductors (TSs) have been a central research topic in present condensed matter physics [1–10]. According to the bulk-boundary correspondence, which is an essential concept in the physics of topological condensed matters, a MZM in a  $d$ -dimensional  $n$ -th order TS is localized at the  $(d-n)$ -dimensional surfaces of the system. In this perspective, the dimensionality and position of the MZM are fully determined by the bulk-boundary correspondence. However, as we show in this Letter, systems with ill-defined dimensions can exhibit exotic MZM that go beyond the framework of the established bulk-boundary correspondence.

Specifically, we predict the emergence of a peculiar MZM that is not localized at one edge of a TS, but splits into multiple parts located at distant edges of different TSs. Hereinafter, we refer to this unconventional zero mode, which holds both the Majorana character and the extreme nonlocality, as a multi-locational Majorana zero mode (MMM). Specifically, as illustrated in Fig. 1(b), we demonstrate the emergence of the MMM in a three-terminal Josephson junction (TJJ) consisting of one-dimensional TSs (hereinafter, referred to as a topological TJJ), which forms an elemental qubit of fault-tolerant topological quantum computers [11–17].

Moreover, we show that the MMM in the TJJ gives rise to dramatic nonlocal resonant transport phenomena, which manifest clearly the coexistence of the Majorana character and the nonlocality. At present, topological TJJs have not yet been experimentally realized. Nevertheless, on the way to realizing the fault-tolerant topological quantum computations, which is a central goal of the topological condensed matter physics, future experiments will certainly build the topological TJJs. In the near future, the proposed experiment to detect the MMM can play a significant role in demonstrating conclusively the realization of not only the TSs but also the

full functionality of the topological TJJ.

*Multi-locational Majorana zero modes.*—We start with a low-energy effective Hamiltonian describing the couplings between MZMs in a topological TJJ. As illustrated in Fig. 1(a), in the absence of any couplings, one MZM appears at each end of the three TSs, where we denote the Majorana operator for the outer (inner) MZM of the  $\alpha$ -th TS with  $\gamma_{o(i),\alpha} = \gamma_{o(i),\alpha}^\dagger$ . In the TJJ, the couplings between these MZMs are described by

$$H = \frac{1}{2} \gamma^T \mathcal{H} \gamma, \quad \mathcal{H} = \begin{pmatrix} 0_{3 \times 3} & i\mathcal{H}_T \\ -i\mathcal{H}_T & \mathcal{H}_J \end{pmatrix},$$

$$\mathcal{H}_T = \text{diag}[E_{T,1}, E_{T,2}, E_{T,3}],$$

$$\mathcal{H}_J = \begin{pmatrix} 0 & iE_{J,12} & iE_{J,13} \\ -iE_{J,12} & 0 & iE_{J,23} \\ -iE_{J,13} & -iE_{J,23} & 0 \end{pmatrix}. \quad (1)$$

where  $\gamma = [\gamma_{o,1}, \gamma_{o,2}, \gamma_{o,3}, \gamma_{i,1}, \gamma_{i,2}, \gamma_{i,3}]^T$ . The  $3 \times 3$  null matrix is represented by  $0_{3 \times 3}$ . The couplings between the outer and inner MZMs of the  $\alpha$ -th TS are characterized by  $E_{T,\alpha} \propto \exp(-2L_\alpha/\xi)$  [13, 18], where  $L_\alpha$  and  $\xi$  represent the length of the  $\alpha$ -th TS and the decay length of

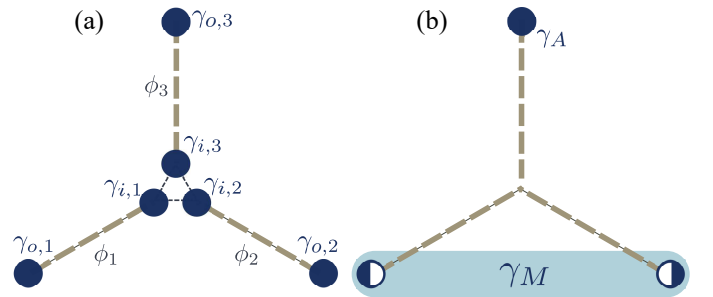


FIG. 1. Schematic image of the topological TJJ. (a) MZMs in the absence of couplings. (b) MZMs with  $v_1, v_2 \ll E_J$  and  $v_3 = 0$ . The MMM is represented by  $\gamma_M$ .

the MZM, respectively. The couplings between the inner MZMs at the Josephson junction is described by  $\mathcal{H}_J$  [2], where  $E_{J,\alpha\beta} = C_{\alpha\beta} \sin[(\phi_\alpha - \phi_\beta)/2]$  with  $C_{\alpha\beta} = C_{\beta\alpha}$  and  $\phi_\alpha$  representing the superconducting phase of the  $\alpha$ -th TS. For simplicity, we ignore long-range couplings, i.e.,  $\gamma_{o,\alpha}$  couples only with  $\gamma_{i,\alpha}$ .

Since  $\mathcal{H}_J$  is a  $3 \times 3$  skew-symmetric matrix, it always has an unpaired zero-eigenvalue, where the two finite eigenvalues are given by  $\pm E_J$  with  $E_J = \sqrt{E_{J,12}^2 + E_{J,23}^2 + E_{J,31}^2}$  [19]. By applying a unitary transformation to diagonalize  $\mathcal{H}_J$ , as also shown in the Supplemental Material (SM) [20], we rewrite the Hamiltonian as

$$H = \frac{1}{2} \tilde{\gamma}^\dagger \begin{pmatrix} \mathcal{H}_{\text{eff}} & \mathcal{V} \\ \mathcal{V}^\dagger & \mathcal{E}_J \end{pmatrix} \tilde{\gamma}, \quad (2)$$

$$\mathcal{H}_{\text{eff}} = \begin{pmatrix} 0 & 0 & 0 & iv_1 \\ 0 & 0 & 0 & iv_2 \\ 0 & 0 & 0 & iv_3 \\ -iv_1 & -iv_2 & -iv_3 & 0 \end{pmatrix},$$

$$\mathcal{V} = \begin{pmatrix} iv_{1,+} & iv_{1,-} \\ iv_{2,+} & iv_{2,-} \\ iv_{3,+} & iv_{3,-} \\ 0 & 0 \end{pmatrix}, \quad \mathcal{E}_J = \begin{pmatrix} E_J & 0 \\ 0 & -E_J \end{pmatrix},$$

where  $\tilde{\gamma} = [\gamma_{o,1}, \gamma_{o,2}, \gamma_{o,3}, \gamma_{0,J}, \gamma_{+,J}, \gamma_{-,J}]^T$ , with  $\gamma_{0,J}$  and  $\gamma_{\pm,J}$  corresponding to the zero-energy eigenstate and the finite-energy eigenstates of  $\mathcal{H}_J$ , respectively. Specifically, we obtain

$$v_\alpha = E_{T,\alpha} \sum_{\beta,\gamma} \epsilon^{\alpha\beta\gamma} \frac{E_{J,\beta\gamma}}{2E_J}, \quad (3)$$

where  $\epsilon^{\alpha\beta\gamma}$  is the Levi-Civita symbol, and the components in  $\mathcal{V}$  are also of the order of  $E_{T,\alpha}$ . Thus, in the limit of  $E_T \ll E_J$  with  $E_T = \sqrt{E_{T,1}^2 + E_{T,2}^2 + E_{T,3}^2}$ , the low-energy excitation of  $|E| \ll E_J$  is approximately described by [21, 22],

$$H_{\text{eff}} = \frac{1}{2} \gamma_{\text{eff}}^T \mathcal{H}_{\text{eff}} \gamma_{\text{eff}}, \quad (4)$$

$$\gamma_{\text{eff}} = [\gamma_{o,1}, \gamma_{o,2}, \gamma_{o,3}, \gamma_{0,J}]^T,$$

where the contributions from the finite-energy eigenstates at the Josephson junction, described by  $\gamma_{\pm,J}$ , are ignored. The detailed discussion on the validity of  $H_{\text{eff}}$  is presented in the SM [20]. The effective low-energy Hamiltonian  $H_{\text{eff}}$  always has doubly degenerate MZMs:

$$\gamma_n = \sum_{\alpha=1-3} c_\alpha^n \gamma_{o,\alpha} \quad (n=1,2), \quad (5)$$

where the real-number coefficients  $c_\alpha^n$  satisfy

$$\sum_\alpha v_\alpha c_\alpha^n = 0, \quad \sum_\alpha c_\alpha^n c_\alpha^m = \delta_{m,n}. \quad (6)$$

Remarkably, one or two of the MZMs in the topological TJJ (i.e.,  $\gamma_n$ ) must be described by the superposition of the outer end MZMs (i.e.,  $\gamma_{o,\alpha}$ ). Thus, the wave function of  $\gamma_n$  has a multi-locational character in which the amplitude is split into parts localized at the outer edges of different TSs. This exceptionally nonlocal MZM is what we refer to as the MMM.

To be more specific, we assume  $v_3 = 0$ , which is realized when the length of the third TS is long enough as  $L_3 \gg \xi$  (i.e.,  $E_{T,3} = 0$ ) or when the first and second TSs have the same phase with respect to the third one, e.g.,  $(\phi_1, \phi_2, \phi_3) = (0, 0, \delta\phi)$  (i.e.,  $E_{J,12} = 0$ ). In this case, we obtain

$$H_{\text{eff}} = \frac{1}{2} \tilde{\gamma}_{\text{eff}}^T \begin{pmatrix} 0 & 0 & iv_1 \\ 0 & 0 & iv_2 \\ -iv_1 & -iv_2 & 0 \end{pmatrix} \tilde{\gamma}_{\text{eff}}, \quad (7)$$

where  $\tilde{\gamma}_{\text{eff}} = [\gamma_{o,1}, \gamma_{o,2}, \gamma_{0,J}]^T$ . The MZM of  $\gamma_A = \gamma_{o,3}$  does not enter the Hamiltonian due to  $v_3 = 0$ , which means that an isolated MZM exist at the outer end of the third TS, as illustrated in Fig. 1(b). More importantly, we again obtain the  $3 \times 3$  skew-symmetric matrix which guarantees the existence of the zero-energy eigenstate:

$$\gamma_M = c_1 \gamma_{o,1} + c_2 \gamma_{o,2}, \quad (8)$$

$$c_1 = \frac{v_2}{\sqrt{v_1^2 + v_2^2}}, \quad c_2 = \frac{-v_1}{\sqrt{v_1^2 + v_2^2}}.$$

As also illustrated in Fig. 1(b), the MMM of  $\gamma_M$  has the amplitudes at two distant places, i.e., the outer edges of the first and second TSs.

*Transport anomalies.*—Here we examine transport anomalies due to the MMM at  $v_1, v_2 \neq 0$  and  $v_3 = 0$  (i.e.,  $\gamma_M$ ). To capture the essence, we first study analytically the transport properties by using the coupling Hamiltonian in Eq. (23). Then, we numerically reproduce the analytical results by employing an explicit model for the topological TJJ, where the TSs are describe by the tight-binding Bogoliubov-de Gennes (BdG) Hamiltonian for a spin-less  $p$ -wave superconductor (i.e., Kitaev chain [2]).

To study the transport properties of the MMM, we attach a normal-metal lead to the outer end of each TS, where we refer to the lead attached to the  $\alpha$ -th TS as the  $\alpha$ -th lead. For the wide-bandwidth normal-metal leads, the scattering matrix at energy  $E$  is generally represented by [23–25]

$$S(E) = \begin{pmatrix} s_{ee}^{ee} & s_{ee}^{eh} \\ s_{he}^{he} & s_{he}^{hh} \end{pmatrix} \quad (9)$$

$$= 1 - 2\pi i W^\dagger [E - \mathcal{H} + i\pi W W^\dagger]^{-1} W,$$

where  $(s^{\eta\zeta})_{\alpha\beta} = s_{\alpha\beta}^{\eta\zeta}$  with  $s_{\alpha\beta}^{ee}$  and  $s_{\alpha\beta}^{he}$  ( $s_{\alpha\beta}^{eh}$  and  $s_{\alpha\beta}^{hh}$ ) representing the scattering coefficients from the electron (hole) in the  $\beta$ -th lead to the electron and hole in the  $\alpha$ -th lead, respectively. In our case, the coupling matrix

$W$  is given by [23]

$$W = \begin{pmatrix} w & -w \\ 0_{3 \times 3} & 0_{3 \times 3} \end{pmatrix}, \quad w = \begin{pmatrix} w_1 & 0 & 0 \\ 0 & w_2 & 0 \\ 0 & 0 & w_3 \end{pmatrix}, \quad (10)$$

where the basis for the normal-metal leads is chosen as  $\mathbf{c} = [c_{e,1}, c_{e,2}, c_{e,3}, c_{h,1}, c_{h,2}, c_{h,3}]^T$  with  $c_{e(h),\alpha}$  representing a propagating electron (hole) in the  $\alpha$ -th lead.  $w_\alpha$  characterizes the couplings between the electron/hole in the  $\alpha$ -th lead and the MZM at the outer end of the  $\alpha$ -th TS. Without loss of generality, we set  $w_\alpha$  to be real numbers [23]. For later convenience, we define

$$\Gamma_{1(2)} = 2\pi c_{1(2)}^2 w_{1(2)}^2, \quad \Gamma_3 = 2\pi w_3^2, \quad (11)$$

where  $\Gamma_\alpha$  characterizes the transparency at the  $\alpha$ -th interfaces. In the presence of the MMM with  $v_3 = 0$ , the scattering coefficients at low energies with low transparency interfaces (i.e.,  $E, \Gamma_\alpha \ll v_1, v_2 \ll E_J$ ) are given by,

$$\begin{aligned} s_{11(22)}^{ee} &= \frac{E + i\Gamma_{1(2)}}{E + i(\Gamma_1 + \Gamma_2)}, \quad s_{11(22)}^{he} = \frac{i\Gamma_{1(2)}}{E + i(\Gamma_1 + \Gamma_2)}, \\ s_{12(21)}^{ee} &= -s_{12(21)}^{he} = \frac{-i\sqrt{\Gamma_1\Gamma_2}}{E + i(\Gamma_1 + \Gamma_2)}, \end{aligned} \quad (12)$$

and

$$\begin{aligned} s_{33}^{ee} &= \frac{E}{E + i\Gamma_3}, \quad s_{33}^{he} = \frac{i\Gamma_3}{E + i\Gamma_3}, \\ s_{\alpha 3}^{ee} &= s_{\alpha 3}^{he} = s_{3\alpha}^{ee} = s_{3\alpha}^{he} = 0, \quad (\alpha \neq 3), \end{aligned} \quad (13)$$

where the detailed derivation for the scattering coefficients are shown in the SM [20]. At zero energy, the isolated MZM of  $\gamma_A$  causes a local resonant Andreev reflection (i.e.,  $|s_{33}^{he}|^2 = 1$ ). More importantly, the scatterings in the first and second leads show highly intertwined properties: at zero-energy, the local normal (Andreev) reflection probability in the first lead is consistent with the local Andreev (normal) reflection probability in the second lead (i.e.,  $|s_{11}^{ee}|^2 = |s_{22}^{he}|^2$  and  $|s_{22}^{ee}|^2 = |s_{11}^{he}|^2$ ), and all nonlocal scattering probabilities between the first and second leads are equivalent (i.e.,  $|s_{12}^{ee}|^2 = |s_{12}^{he}|^2 = |s_{21}^{ee}|^2 = |s_{21}^{he}|^2$ ). The entangled scatterings with respect to the first and second leads are obviously due to the MMM, whose wave function amplitude is split between the first and second TSs.

Then, we describe how the entangled scatterings of the MMM affect charge transport phenomena. For this purpose, we apply the same bias voltage  $V$  to all normal-metal leads, while all TSs are grounded. We assume significantly low transparency at the interfaces between the leads and TSs, such that the bias voltages applied to the leads are dropped only at the interfaces. We also assume  $(\phi_1, \phi_2, \phi_3) = (0, 0, \pi)$ , such that the Josephson currents between the TSs are absent; this assumption yields  $v_3 = 0$ , and thus we obtain  $\gamma_M$  in Eq. (48).

Within the Blonder–Tinkham–Klapwijk (BTK) formalism, the differential conductance  $G_\alpha(eV) = dI_\alpha/dV$  at zero-temperature is given by [26, 27]

$$G_\alpha(eV) = \frac{e^2}{h} \sum_j [\delta_{\alpha\beta} - |s_{\alpha\beta}^{ee}|^2 + |s_{\alpha\beta}^{he}|^2]_{E=eV}, \quad (14)$$

where  $I_\alpha$  is the time-averaged current in the  $\alpha$ -th lead. We note that our calculations based on the BTK formalism is qualitatively justified for bias voltages well below the superconducting gap. The differential conductance at low bias voltages with low transparency interfaces (i.e.,  $eV, \Gamma_\alpha \ll v_1, v_2 \ll E_J$ ) is given by

$$\begin{aligned} G_{1(2)} &= \frac{2e^2}{h} \frac{\Gamma_{1(2)}(\Gamma_1 + \Gamma_2)}{E^2 + (\Gamma_1 + \Gamma_2)^2} \Big|_{E=eV}, \\ G_3 &= \frac{2e^2}{h} \frac{\Gamma_3^2}{E^2 + \Gamma_3^2} \Big|_{E=eV}. \end{aligned} \quad (15)$$

The differential conductance of the third lead exhibits the zero-bias conductance quantization, i.e.,  $G_3(0) = 2e^2/h$  [28–32]. On the other hand,  $G_1(0)$  and  $G_2(0)$  depend on the transparency of the interfaces and are not quantized. Nevertheless, a remarkable relation always holds:

$$G_1(0) + G_2(0) = \frac{2e^2}{h}. \quad (16)$$

Namely, the sum of zero-bias differential conductance in the significantly distant leads is perfectly quantized. The observation of the nonlocally quantized conductance, which cannot occur in the absence of the MMM, can be a smoking-gun evidence for the realization of the fully functional topological TJJ.

Even though the current shot noise is more difficult to measure experimentally than the differential conductance, it also manifests the profound nature of entangle scatterings of the MMM. Here we specifically discuss the zero-frequency noise power defined by

$$P_{\alpha\beta} = \int_{-\infty}^{\infty} \overline{\delta I_\alpha(0) \delta I_\beta(t)} dt, \quad (17)$$

where  $\delta I_\alpha(t) = I_\alpha(t) - I_\alpha$  denotes the deviation of the current at time  $t$  from the time averaged current. Within the BTK formalism, the zero-frequency noise power at zero-temperature is given by [33, 34]

$$\begin{aligned} P_{\alpha\beta} &= \frac{e^2}{h} \int_0^{eV} \mathcal{P}_{\alpha\beta}(E) dE, \\ \mathcal{P}_{\alpha\beta}(E) &= \delta_{\alpha\beta} \sum_{\eta=e,h} p_{\alpha\alpha}^{\eta\eta} - \sum_{\eta,\zeta} \sigma_\eta \sigma_\zeta p_{\alpha\beta}^{\eta\zeta} p_{\beta\alpha}^{\zeta\eta}, \\ p_{\alpha}^{\eta\zeta} &= \sum_{\gamma=1,2,3} s_{\alpha\gamma}^{\eta e} (s_{\beta\gamma}^{\zeta e})^*, \end{aligned} \quad (18)$$

where  $\sigma_\eta = 1$  ( $-1$ ) for  $\eta = e$  ( $h$ ). For significantly low bias voltages with low transparency interfaces, such as

$eV \ll \Gamma_\alpha \ll v_1, v_2 \ll E_J$ , the zero-frequency noise power is given by

$$\begin{aligned} P_{11} &= P_{22} = -P_{12} = -P_{21} = \frac{2h}{eV} I_1 I_2, \\ P_{33} &= P_{3\alpha} = P_{\alpha 3} = 0, \quad (\alpha \neq 3), \end{aligned} \quad (19)$$

where we approximate  $P_{\alpha\beta} \approx (e^3 V/h) \mathcal{P}_{\alpha\beta}(0)$  and  $I_\alpha \approx G_{\alpha\alpha}(0)V$ , which is justified in the linear response regime of  $eV \ll \Gamma_\alpha$ . We find that the particular relation,

$$2|P_{12}| = P_{11} + P_{22}, \quad (20)$$

is satisfied, where the cross-correlator in any stochastic processes is bounded by the auto-correlator as  $2|P_{12}| \leq P_{11} + P_{22}$ . Thus, the maximized cross-correlator of  $|P_{12}|$  implies that the MMM causes the perfect correlation between the first and second leads. In addition, the total noise power satisfies  $\sum_{\alpha,\beta} P_{\alpha\beta} = 0$ , which implies that the total charge current flowing into the TSs is noiseless due to the resonant transmissions of the isolated MZM  $\gamma_A$  and the MMM  $\gamma_M$ . Especially, the relation of

$$P_{11} + P_{22} + P_{12} + P_{21} = 0 \quad (21)$$

is closely related with the nonlocally quantized conductance in Eq. (16); both are the physical consequence of the highly entangled resonant scatterings involving the distinctly distant two leads, which are inherently caused by the MMM.

*Numerical results.*—Lastly, we numerically reproduce the dramatic transport anomalies of the MMM by using an explicit BdG Hamiltonian for the topological TJJ. Specifically, we employ the Kitaev chain [2] to describe the TSs. We note that the low-energy physics of various one-dimensional TSs [35], such as superconducting semiconductor nanowire [36–40], magnetic atom chains deposited on superconductors [41–44], and planer topological Josephson junctions [45–53], are described effectively by the Kitaev chain [40, 41, 53]. The BdG Hamiltonian reads  $H_{\text{BdG}} = \sum_{\alpha=1-3} H_\alpha + H_d$  with

$$\begin{aligned} H_\alpha &= \sum_{n_\alpha=-\infty}^{L_\alpha-1} (-t_{n_\alpha} c_{n_\alpha+1}^\dagger c_{n_\alpha} + \text{h.c.}) - \sum_{n_\alpha=-\infty}^{L_\alpha} \mu c_{n_\alpha}^\dagger c_{n_\alpha} \\ &\quad + \frac{1}{2} \sum_{n_\alpha=1}^{L_\alpha-1} (i\Delta e^{i\phi_\alpha} c_{n_\alpha+1}^\dagger c_{n_\alpha}^\dagger + \text{h.c.}), \\ H_d &= -t_d \sum_{\alpha=1-3} (c_d^\dagger c_{L_\alpha} + \text{h.c.}) - \mu_d c_d^\dagger c_d, \end{aligned} \quad (22)$$

where  $c_{n_\alpha}$  ( $c_{n_\alpha}^\dagger$ ) is the annihilation (creation) operator of an electron at a site  $n_\alpha$  of the  $\alpha$ -th branch,  $t_{n_\alpha}$  is the nearest-neighbor hopping integral,  $\mu$  denotes the chemical potential, and  $\Delta$  represents the pair potential in the superconducting segment. The interface between the normal-metal lead and the superconductor is located at  $n_\alpha = 0$ , where we set  $t_{n_\alpha} = t$  for  $n_\alpha \neq 0$  and  $t_{n_\alpha} = t'_\alpha$  at

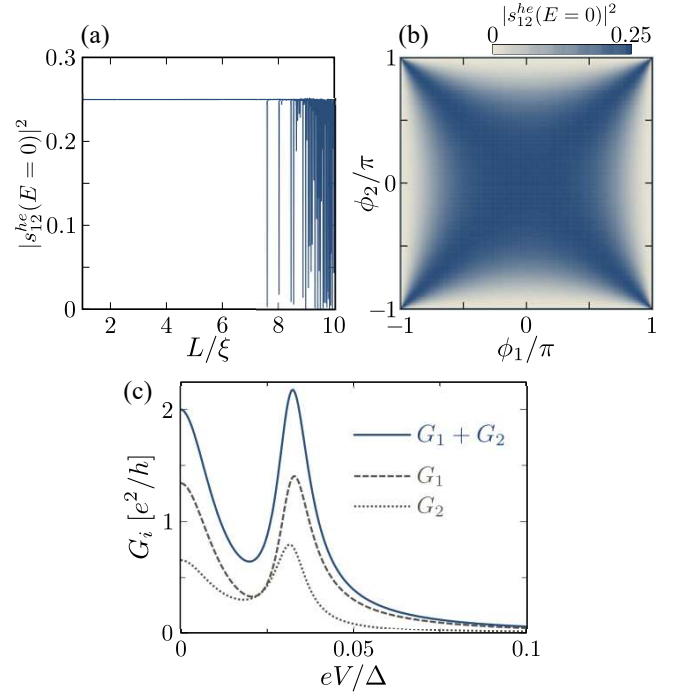


FIG. 2. Nonlocal Andreev reflection probability of  $|s_{12}^{he}|^2$  at zero energy (a) as a function of the superconductor length and (b) as a function of the superconducting phases. (c) Differential conductance as a function of the bias voltage.

$n_\alpha = 0$ . The three TSs are connected through a single normal site, where the coupling is described by  $H_d$ . We numerically compute the scattering coefficients using lattice Green's function techniques [54, 55]. In the following calculations, we fix the parameters as  $\mu = \mu_d = -0.8t$ ,  $t_d = t$ , and  $\Delta = 0.01t$ , where the decay length of MZMs is evaluated by  $\xi = \arctan^{-1}(\Delta/2t) \approx 200$ . To focus on the transport properties of  $\gamma_M$ , we fix the length of the third TS as  $L_3 = 2000 \approx 10\xi$ , which is sufficiently longer than the decay length of MZMs. For simplicity, we also assume that the first and second TSs have the same length  $L_1 = L_2 = L$ .

In Fig. 2(a), we show the nonlocal Andreev reflection probability of  $|s_{12}^{he}|^2$  at zero energy as a function of the superconductor length  $L$ . We consider a low-transparency junction with  $t'_\alpha = 0.05t$ . The superconducting phases are chosen as  $(\phi_1, \phi_2, \phi_3) = (0, 0, \pi)$ . We clearly find the plateau at  $|s_{12}^{he}|^2 = 1/4$  in the broad range of  $L$ , which agrees with Eq. (12) at  $\Gamma_1 = \Gamma_2$ . In the SM [20], we also confirm that at the plateau, other scattering amplitudes also show the excellent agreement with Eq. (12). For longer  $L$  exceeding  $7\xi$ , we see the deviation from  $|s_{12}^{he}|^2 = 1/4$ . This is because the condition of  $E, \Gamma_\alpha \ll v_1, v_2$ , which justifies Eq. (12), is no longer satisfied, where  $E_{T,\alpha} \approx \Delta \cos(k_F L) e^{-2L_\alpha/\xi}$  with  $k_F = \arccos(\mu/2t)$  [18], and thus  $v_\alpha$ , oscillates and decays by increasing  $L$ . Nevertheless, it has been shown



that typical nonlocal scatterings through superconductors decay exponentially with the distance between the leads on a scale fixed by  $\xi$  [23–25]. We remark that the first and second leads are separated by two TSs with the length  $L$ . Namely, in the TJJ, the relation of  $|s_{12}^{he}|^2 = 1/4$  is maintained even when the distance between the two leads (i.e.,  $2L$ ) exceeds  $10\xi$ . As a result, the long-range plateau in Fig. 2(a) proves the dramatic nonlocal resonant scatterings of the MMM within the tight-binding model. In Fig. 2(b), we show  $|s_{12}^{he}|^2$  at zero energy as a function of the superconductor phases of  $\phi_1$  and  $\phi_2$ , where we fix  $\phi_3 = \pi$ . The length of the superconducting segment is chosen as  $L = 800 \approx 4\xi$ . We find the large nonlocal Andreev reflection of  $|s_{12}^{he}|^2 \sim 1/4$  in the broad range of  $(\phi_1, \phi_2)$  except around  $\phi_{1(2)} = \pm\pi$  yielding  $v_{2(1)} = 0$ . In Fig. 2(c), we show the differential conductance at  $L = 800 \approx 4\xi$  as a function of the bias voltage, where we choose  $(\phi_1, \phi_2, \phi_3) = (0, 0, \pi)$  and  $(t'_1, t'_2, t'_3) = (0.07t, 0.1t, 0.07t)$ . While  $G_1 \neq G_2$  owing to  $t'_1 \neq t'_2$ , we see  $G_1 + G_2$  at zero-bias voltage is quantized to  $2e^2/h$ . Therefore, we numerically demonstrate the nonlocally quantized conductance of the MMM. We also find the second peak at the finite bias voltage approximately given by  $eV \approx \sqrt{v_1^2 + v_2^2}$ , which characterizes the necessary resolutions in experiments. Nevertheless, we remark that in the artificial TSs [36–53], the coupling strength  $E_{T,\alpha}$ , as well as the decay length of the MZM, can be controlled, for example, by changing applied Zeeman fields [18]. In the SM [20], we also demonstrate the anomalies in the current shot noise (i.e. Eq. (20) and Eq. (21)) within the tight-binding model.

*Discussion.*—In this paper, we discuss the charge currents only when the Josephson currents are absent, i.e., the superconducting phases are fixed at  $(\phi_1, \phi_2, \phi_3) = (0, 0, \pi)$ . Studying other various cases, for example, the coexistence of charge currents due to the bias voltages and Josephson currents [56–58], remains as an important future task. Nevertheless, we still expect dramatic transport anomalies because as shown in Eq. (5), the topological TJJ hosts the MMM insensitive to the superconducting phases.

We have shown that MMM in the TJJ can be created when an odd number of MZMs are brought into contact and coupled to each other. Moreover, our analysis is based on an effective Hamiltonian, which focuses just on the couplings between the MZMs and is irrelevant to the details of the parent TS. Thus, we expect that our strategy for creating a MMM can be extended to other systems such as higher-order TSs exhibiting high controllability for the number and location of MZMs [59–62]. We hope that our work will stimulate further theoretical investigations into the anomalous characteristics emerged in systems with an odd number of coupled MZMs, i.e., the systems hosting MMMs. For instance, inspired by the various studies on the conventional MZMs, studying the Cooper pair splittings due to the nonlocal Andreev reflec-

tions [23, 63, 64], the nonlocal Josephson effects forming Cooper quartets [65–67], the quantum teleportation [68–70], and the full-counting statistics [71–73] in the presence of MMMs would be intriguing topics for future work.

In summary, we demonstrate the emergence of the MMM that go beyond the framework of the bulk-boundary correspondence. Thanks to the coexistence of the Majorana character and the extreme nonlocality, the MMM causes prominent nonlocal resonant transport phenomena. We expect that our proposal can be used to prove conclusively the realization of the topological TJJ, which forms an elemental qubit for fault-tolerant topological quantum computers.

S.I. is supported by the Grant-in-Aid for JSPS Fellows (JSPS KAKENHI Grant No. JP22KJ1507).

---

\* These authors contributed equally to this work.

- [1] N. Read and D. Green, Phys. Rev. B **61**, 10267 (2000).
- [2] A. Y. Kitaev, Phys. Usp. **44**, 131 (2001).
- [3] F. Wilczek, Nat. Phys. **5**, 614-618 (2009).
- [4] M. Z. Hasan and C. L. Kane, Rev. Mod. Phys. **82**, 3045 (2010).
- [5] X.-L. Qi and S.-C. Zhang, Rev. Mod. Phys. **83**, 1057 (2011).
- [6] M. Leijnse and K. Flensberg, Semicond. Sci. Technol. **27**, 124003 (2012).
- [7] Y. Tanaka, M. Sato, and N. Nagaosa, J. Phys. Soc. Jpn. **81**, 011013 (2012).
- [8] C. W. J. Beenakker, Annu. Rev. Condens. Matter Phys. **4**, 113-136 (2013).
- [9] M. Sato and S. Fujimoto, J. Phys. Soc. Jpn. **85**, 072001 (2016).
- [10] M. Sato and Y. Ando, Rep. Prog. Phys. **80**, 076501 (2017).
- [11] D. A. Ivanov, Phys. Rev. Lett. **86**, 268 (2001).
- [12] A. Y. Kitaev, Ann. Phys. **303**, 2-30 (2003).
- [13] C. Nayak, S. H. Simon, A. Stern, M. Freedman, and S. DasSarma, Rev. Mod. Phys. **80**, 1083(2008).
- [14] D. Aasen, M. Hell, R. V. Mishmash, A. Higginbotham, J. Danon, M. Leijnse, T. S. Jespersen, J. A. Folk, C. M. Marcus, K. Flensberg, and J. Alicea, Phys. Rev. X **6**, 031016 (2016).
- [15] J. Alicea, Y. Oreg, G. Refael, F. v. Oppen, and M. P. A. Fisher, Nat. Phys. **7**, 412-417(2011).
- [16] J. D. Sau, D. J. Clarke, and S. Tewari, Phys. Rev. B **84**, 094505 (2011).
- [17] S. DasSarma, M. Freedman, and C. Nayak, npj Quantum Information **1**, 15001(2015).
- [18] S. DasSarma, J. D. Sau, and T. D. Stanescu, Phys. Rev. B **86**, 220506(R) (2012).
- [19] K. Sakurai, M. T. Mercaldo, S. Kobayashi, A. Yamakage, S. Ikegaya, T. Habe, P. Kotetes, M. Cuoco, and Y. Asano, Phys. Rev. B **101**, 174506 (2020).
- [20] See Supplemental Material at XXX for the detailed derivation for Eq. (48), Eq. (12), and Eq. (13). We also show the numerical results on the scattering coefficients and the current shot noise.
- [21] J. W. F. Venderbos, L. Savary, J. Ruhman, P. A. Lee,

- and L. Fu, Phys. Rev. X **8**, 011029 (2018).
- [22] P. M. R. Brydon, D. F. Agterberg, Henri Menke, and C. Timm, Phys. Rev. B **98**, 224509 (2018).
- [23] J. Nilsson, A. R. Akhmerov, and C. W. J. Beenakker, Phys. Rev. Lett. **101**, 120403 (2008).
- [24] J. Liu, F.-C. Zhang, and K. T. Law, Phys. Rev. B **88**, 064509 (2013).
- [25] J. Danon, A. B. Hellenes, E. B. Hansen, L. Casparis, A. P. Higginbotham, and K. Flensberg, Phys. Rev. Lett. **124**, 036801 (2020).
- [26] G. E. Blonder, M. Tinkham, and T. M. Klapwijk, Phys. Rev. B **25**, 4515 (1982).
- [27] G. Deutscher and D. Feinberg, Appl. Phys. Lett. **76**, 487-489 (2000).
- [28] Y. Tanaka and S. Kashiwaya, Phys. Rev. Lett. **74**, 3451 (1995).
- [29] K. Sengupta, I. Žutić, H.-J. Kwon, V. M. Yakovenko, and S. DasSarma, Phys. Rev. B **63**, 144531 (2001).
- [30] Y. Tanaka and S. Kashiwaya, Phys. Rev. B **70**, 012507 (2004).
- [31] Y. Tanaka, S. Kashiwaya, and T. Yokoyama, Phys. Rev. B **71**, 094513 (2005).
- [32] K. T. Law, P. A. Lee, and T. K. Ng, Phys. Rev. Lett. **103**, 237001 (2009).
- [33] M. J. M. de Jong and C. W. J. Beenakker, Phys. Rev. B **49**, 16070 (1994).
- [34] M. P. Anantram and S. Datta, Phys. Rev. B **53**, 16390 (1996).
- [35] K. Flensberg, F. v. Oppen, and A. Stern, Nat. Rev. Mater. **6**, 944 (2021).
- [36] R. M. Lutchyn, J. D. Sau, and S. DasSarma, Phys. Rev. Lett. **105**, 077001 (2010).
- [37] Y. Oreg, G. Refael, and F. von Oppen, Phys. Rev. Lett. **105**, 177002 (2010).
- [38] V. Mourik, K. Zuo, S. M. Frolov, S. R. Plissard, E. P. A. M. Bakkers, L. P. Kouwenhoven, Science **336**, 1003-1007 (2012).
- [39] M. T. Deng, C. L. Yu, G. Y. Huang, M. Larsson, P. Caroff, and H. Q. Xu, Nano Lett. **12**, 6414-6419 (2012).
- [40] Y. Asano and Y. Tanaka, Phys. Rev. B **87**, 104513 (2013).
- [41] T.-P. Choy, J. M. Edge, A. R. Akhmerov, and C. W. J. Beenakker, Phys. Rev. B **84**, 195442 (2011).
- [42] S. Nadj-Perge, I. K. Drozdov, B. A. Bernevig, and A. Yazdani, Phys. Rev. B **88**, 020407(R) (2013).
- [43] S. Nadj-Perge, I. K. Drozdov, J. Li, H. Chen, S. Jeon, J. Seo, A. H. MacDonald, B. A. Bernevig, and A. Yazdani, Science **346**, 602-607 (2014).
- [44] B. E. Feldman, M. T. Randeria, J. Li, S. Jeon, Y. Xie, Z. Wang, I. K. Drozdov, B. A. Bernevig, and A. Yazdani, Nat. Phys. **13**, 286-291 (2017).
- [45] M. Hell, M. Leijnse, and K. Flensberg, Phys. Rev. Lett. **118**, 107701 (2017).
- [46] F. Pientka, A. Keselman, E. Berg, A. Yacoby, A. Stern, and B. I. Halperin, Phys. Rev. X **7**, 021032 (2017).
- [47] A. Haim and A. Stern, Phys. Rev. Lett. **122**, 126801 (2019).
- [48] F. Setiawan, A. Stern, and E. Berg, Phys. Rev. B **99**, 220506(R) (2019).
- [49] A. Fornieri, A. M. Whiticar, F. Setiawan, E. Portolés, A. C. C. Drachmann, A. Keselman, S. Gronin, C. Thomas, T. Wang, R. Kallagher, G. C. Gardner, E. Berg, M. J. Manfra, A. Stern, C. M. Marcus, and F. Nichele, Nature **569**, 89-92 (2019).
- [50] H. Ren, F. Pientka, S. Hart, A. T. Pierce, M. Kosowsky, L. Lunczer, R. Schlereth, B. Scharf, E. M. Hankiewicz, L. W. Molenkamp, B. I. Halperin, and A. Yacoby, Nature **569**, 93-98 (2019).
- [51] T. Zhou, M. C. Dartiaillh, W. Mayer, J. E. Han, A. Matos-Abiague, J. Shabani, and I. Žutić, Phys. Rev. Lett. **124**, 137001 (2020).
- [52] M. C. Dartiaillh, W. Mayer, J. Yuan, K. S. Wickramasinghe, A. Matos-Abiague, I. Žutić, and J. Shabani, Phys. Rev. Lett. **126**, 036802 (2021).
- [53] D. Oshima, S. Ikegaya, A. P. Schnyder, and Y. Tanaka, Phys. Rev. Research **4**, L022051 (2022).
- [54] P. A. Lee and D. S. Fisher, Phys. Rev. Lett. **47**, 882 (1981).
- [55] T. Ando, Phys. Rev. B **44**, 8017 (1991).
- [56] O. Deb, K. Sengupta, and D. Sen, Phys. Rev. B **97**, 174518 (2018).
- [57] T. Jonckheere, J. Rech, A. Zazunov, R. Egger, A. L. Yeyati, and T. Martin, Phys. Rev. Lett. **122**, 097003 (2019).
- [58] J. S. Meyer and M. Houzet, Phys. Rev. B **103**, 174504 (2021).
- [59] G. E. Volovik, JETP Lett. **91**, 201-205 (2010).
- [60] X. Zhu, Phys. Rev. B **97**, 205134 (2018).
- [61] Z. Yan, F. Song, and Z. Wang, Phys. Rev. Lett. **121**, 096803 (2018).
- [62] S. Ikegaya, W. B. Rui, D. Manske, and A. P. Schnyder, Phys. Rev. Research **3**, 023007 (2021).
- [63] J. J. He, J. Wu, T.-P. Choy, X.-J. Liu, Y. Tanaka, and K. T. Law, Nat. Commun. **5**, 3232 (2014).
- [64] T. Ö. Rosdahl, A. Vuik, M. Kjaergaard, and A. R. Akhmerov, Phys. Rev. B **97**, 045421 (2018).
- [65] A. Freyn, Benoit Douçot, D. Feinberg, and R. Mélin, Phys. Rev. Lett. **106**, 257005 (2011).
- [66] Y. Cohen, Y. Ronen, J.-H. Kang, M. Heiblum, D. Feinberg, R. Mélin, and H. Shtrikman, Proc. Natl. Acad. Sci. U.S.A. **115**, 6991-6994 (2018).
- [67] J.-D. Pillet, V. Benzoni, J. Griesmar, J.-L. Smirr, and Ç. Ö. Girit, Nano Lett. **19**, 7138-7143 (2019).
- [68] L. Fu, Phys. Rev. Lett. **104**, 056402 (2010).
- [69] A. Zazunov, A. L. Yeyati, and R. Egger, Phys. Rev. B **84**, 165440 (2011).
- [70] R. Hütten, A. Zazunov, B. Braunecker, A. L. Yeyati, and R. Egger, Phys. Rev. Lett. **109**, 166403 (2012).
- [71] L. Weithofer, P. Recher, and T. L. Schmidt, Phys. Rev. B **90**, 205416 (2014).
- [72] D. E. Liu, A. Levchenko, and R. M. Lutchyn, Phys. Rev. B **92**, 205422 (2015).
- [73] N. V. Gnezdilov, B. van Heck, M. Diez, J. A. Hutasoit, and C. W. J. Beenakker, Phys. Rev. B **92**, 121406(R) (2015).

## Supplemental Material for “Multi-locational Majorana Zero Modes”

Yutaro Nagae<sup>1</sup>, Andreas P. Schnyder<sup>2</sup>, Yukio Tanaka<sup>1</sup>, Yasuhiro Asano<sup>3</sup>, and Satoshi Ikegaya<sup>1,4</sup>

<sup>1</sup>*Department of Applied Physics, Nagoya University, Nagoya 464-8603, Japan*

<sup>2</sup>*Max-Planck-Institut für Festkörperforschung, Heisenbergstrasse 1, D-70569 Stuttgart, Germany*

<sup>3</sup>*Department of Applied Physics, Hokkaido University, Sapporo 060-8628, Japan*

<sup>4</sup>*Institute for Advanced Research, Nagoya University, Nagoya 464-8601, Japan*

### LOW-ENERGY EFFECTIVE HAMILTONIAN

In this section, we derive the low-energy effective Hamiltonian for the three-terminal Josephson junctions consisting of the one-dimensional topological superconductors (TSs), which is given by Eq. (4) in the main text. We start with the Hamiltonian in Eq. (1) in the main text, which describes the couplings between Majorana zero modes (MZMs) in the topological three-terminal Josephson junction:

$$\begin{aligned}
 H &= \frac{1}{2} \boldsymbol{\gamma}^T \mathcal{H} \boldsymbol{\gamma}, \\
 \boldsymbol{\gamma} &= [\gamma_{o,1}, \gamma_{o,2}, \gamma_{o,3}, \gamma_{i,1}, \gamma_{i,2}, \gamma_{i,3}]^T, \quad \mathcal{H} = \begin{pmatrix} 0_{3 \times 3} & i\mathcal{H}_T \\ -i\mathcal{H}_T & \mathcal{H}_J \end{pmatrix}, \\
 \mathcal{H}_T &= \text{diag}[E_{T,1}, E_{T,2}, E_{T,3}], \quad \mathcal{H}_J = \begin{pmatrix} 0 & iE_{J,12} & iE_{J,13} \\ -iE_{J,12} & 0 & iE_{J,23} \\ -iE_{J,13} & -iE_{J,23} & 0 \end{pmatrix}.
 \end{aligned} \tag{23}$$

where  $\gamma_{o(i),\alpha} = \gamma_{o(i),\alpha}^\dagger$  is an outer (inner) MZM of the  $\alpha$ -th TS, the coupling constant between the outer and inner MZMs in the  $\alpha$ -th TS is given by  $E_{T,\alpha}$ , and the coupling between the inner MZMs of the  $\alpha$ -th and  $\beta$ -th TSs at the Josephson junction is represented by  $E_{J,\alpha\beta} = -E_{J,\beta\alpha}$ . The  $n \times m$  null matrix is given by  $0_{n \times m}$ . At first, we define a  $3 \times 3$  unitary matrix that diagonalizes  $\mathcal{H}_J$ :

$$\begin{aligned}
 \mathcal{U}_J^\dagger \mathcal{H}_J \mathcal{U}_J &= \begin{pmatrix} 0 & 0_{1 \times 2} \\ 0_{2 \times 1} & \mathcal{E}_J \end{pmatrix}, \\
 \mathcal{E}_J &= \begin{pmatrix} E_J & 0 \\ 0 & -E_J \end{pmatrix}, \quad E_J = \sqrt{E_{J,12}^2 + E_{J,23}^2 + E_{J,31}^2},
 \end{aligned} \tag{24}$$

with

$$\mathcal{U}_J = (\mathbf{V}_0, \mathbf{V}_+, \mathbf{V}_-), \tag{25}$$

where  $\mathbf{V}_0$  and  $\mathbf{V}_\pm$  are the three-element vectors satisfying

$$\mathcal{H}_J \mathbf{V}_0 = 0, \quad \mathcal{H}_J \mathbf{V}_\pm = \pm E_J \mathbf{V}_\pm, \tag{26}$$

respectively. Specifically,  $\mathbf{V}_0$  is given by

$$\mathbf{V}_0 = \frac{1}{E_J} \begin{pmatrix} E_{J,23} \\ -E_{J,13} \\ E_{J,12} \end{pmatrix}. \tag{27}$$

In addition, we define the field operators of

$$\begin{pmatrix} \gamma_{0,J} \\ \gamma_{+,J} \\ \gamma_{-,J} \end{pmatrix} = \mathcal{U}_J^\dagger \begin{pmatrix} \gamma_{i,1} \\ \gamma_{i,2} \\ \gamma_{i,3} \end{pmatrix} \tag{28}$$

where  $\gamma_{0,J}$  and  $\gamma_{\pm,J}$  corresponding to the field operators for the zero-energy eigenstate and the finite-energy eigenstates, respectively. We also note that  $\gamma_{0,J}$  still satisfies the Majorana relation,  $\gamma_{0,J} = \gamma_{0,J}^\dagger$ . By using the  $6 \times 6$  unitary matrix of

$$\mathcal{U} = \begin{pmatrix} 1_3 & 0_{3 \times 3} \\ 0_{3 \times 3} & \mathcal{U}_J \end{pmatrix}, \tag{29}$$

with  $1_n$  being the  $n \times n$  identity matrix, we rewrite the Hamiltonian as

$$H = \frac{1}{2} \gamma^T \mathcal{U} \mathcal{U}^\dagger \mathcal{H} \mathcal{U} \mathcal{U}^\dagger \gamma = \frac{1}{2} \tilde{\gamma}^\dagger \tilde{\mathcal{H}} \tilde{\gamma}, \quad (30)$$

with

$$\tilde{\gamma} = \mathcal{U}^\dagger \gamma = [\gamma_{o,1}, \gamma_{o,2}, \gamma_{o,3}, \gamma_{0,J}, \gamma_{+,J}, \gamma_{-,J}]^T, \quad (31)$$

and

$$\tilde{\mathcal{H}} = \mathcal{U}^\dagger \mathcal{H} \mathcal{U} = \begin{pmatrix} 0_{3 \times 3} & i\mathcal{H}_T \mathcal{U}_J \\ -i\mathcal{U}_J^\dagger \mathcal{H}_T & \mathcal{U}_J^\dagger \mathcal{H}_J \mathcal{U}_J \end{pmatrix}. \quad (32)$$

For later convenience, we further rewrite the Hamiltonian as

$$H = \frac{1}{2} \tilde{\gamma}^\dagger \begin{pmatrix} \mathcal{H}_0 & \mathcal{V} \\ \mathcal{V}^\dagger & \mathcal{E}_J \end{pmatrix} \tilde{\gamma}, \quad (33)$$

$$\mathcal{H}_0 = \begin{pmatrix} 0 & 0 & 0 & iv_1 \\ 0 & 0 & 0 & iv_2 \\ 0 & 0 & 0 & iv_3 \\ -iv_1 & -iv_2 & -iv_3 & 0 \end{pmatrix}, \quad \mathcal{V} = \begin{pmatrix} iv_{1,+} & iv_{1,-} \\ iv_{2,+} & iv_{2,-} \\ iv_{3,+} & iv_{3,-} \\ 0 & 0 \end{pmatrix},$$

where

$$\begin{pmatrix} v_1 \\ v_2 \\ v_3 \end{pmatrix} = \mathcal{H}_T \mathbf{V}_0 = \frac{1}{E_J} \begin{pmatrix} E_{T,1} E_{J,23} \\ -E_{T,2} E_{J,13} \\ E_{T,3} E_{J,12} \end{pmatrix}, \quad (34)$$

and

$$\begin{pmatrix} v_{1,\pm} \\ v_{2,\pm} \\ v_{3,\pm} \end{pmatrix} = \mathcal{H}_T \mathbf{V}_\pm. \quad (35)$$

The Hamiltonian in Eq. (33) is equivalent to that in Eq. (2) of the main text.

To construct the low-energy effective Hamiltonian, we consider the resolvent corresponding to  $\tilde{\mathcal{H}}$  [21, 22]:

$$\mathcal{G}(E) = (E - \tilde{\mathcal{H}})^{-1} = \begin{pmatrix} \mathcal{G}_{\text{mzm}} & \mathcal{G}_\mathcal{V} \\ \mathcal{G}_{\mathcal{V}^\dagger} & \mathcal{G}_J \end{pmatrix}. \quad (36)$$

The block component related to the MZMs of

$$\gamma_{\text{eff}} = [\gamma_{o,1}, \gamma_{o,2}, \gamma_{o,3}, \gamma_{0,J}]^T \quad (37)$$

is obtained as

$$\begin{aligned} \mathcal{G}_{\text{mzm}}(E) &= [E - \mathcal{H}_{\text{mzm}}(E)]^{-1}, \\ \mathcal{H}_{\text{mzm}}(E) &= \mathcal{H}_0 + \mathcal{V}(E - \mathcal{E}_J)^{-1} \mathcal{V}^\dagger. \end{aligned} \quad (38)$$

When we focus on the low-energy excitation of  $|E| \ll E_J$ , we can make the replacement of

$$\mathcal{V}(E - \mathcal{E}_J)^{-1} \mathcal{V}^\dagger \approx -\frac{1}{E_J} \mathcal{V} \begin{pmatrix} 1 & 0 \\ 0 & -1 \end{pmatrix} \mathcal{V}^\dagger, \quad (39)$$

which yields the effective Hamiltonian describing the low-energy excitation of  $|E| \ll E_J$  [21, 22]:

$$\mathcal{H}_{\text{eff}} = \mathcal{H}_0 + \delta\mathcal{H}, \quad \delta\mathcal{H} = -\frac{1}{E_J} \mathcal{V} \begin{pmatrix} 1 & 0 \\ 0 & -1 \end{pmatrix} \mathcal{V}^\dagger. \quad (40)$$



The finite matrix elements in  $\mathcal{H}_0$  are of the order of  $E_T$ , while finite matrix elements in  $\delta\mathcal{H}$  are of the order of  $E_T^2/E_J$ , where  $E_T = \sqrt{E_{T,1}^2 + E_{T,2}^2 + E_{T,3}^2}$ . Therefore, in the limit of  $E_T \ll E_J$ , we can neglect the insignificant terms of  $O(E_T^2/E_J)$  and obtain

$$\mathcal{H}_{\text{eff}} \approx \mathcal{H}_0. \quad (41)$$

Eventually, the effective Hamiltonian describing low-energy excitation of  $|E| \ll E_J$  in the limit of  $E_T \ll E_J$  is obtained by

$$H_{\text{eff}} = \frac{1}{2} \gamma_{\text{eff}}^T \mathcal{H}_{\text{eff}} \gamma_{\text{eff}}, \quad \mathcal{H}_{\text{eff}} = \begin{pmatrix} 0 & 0 & 0 & iv_1 \\ 0 & 0 & 0 & iv_2 \\ 0 & 0 & 0 & iv_3 \\ -iv_1 & -iv_2 & -iv_3 & 0 \end{pmatrix}, \quad (42)$$

which is equivalent to the Hamiltonian in Eq. (4) of the main text. As we discussed in the main text, the effective Hamiltonian of  $H_{\text{eff}}$  exhibits the multi-locational Majorana zero modes (MMMs).

Here we specifically focus on the zero-energy states at  $v_1, v_2 \neq 0$  and  $v_3 = 0$ . The effective Hamiltonian at  $v_1, v_2 \neq 0$  and  $v_3 = 0$  is diagonalized as,

$$\mathcal{U}_{\text{eff}}^\dagger \mathcal{H}_{\text{eff}} \mathcal{U}_{\text{eff}} = \mathcal{E}_{\text{eff}} = \text{diag}[0, 0, v, -v], \quad v = \sqrt{v_1^2 + v_2^2}, \quad (43)$$

with

$$\mathcal{U}_{\text{eff}} = (\mathbf{u}_A, \mathbf{u}_M, \mathbf{u}_+, \mathbf{u}_-), \quad (44)$$

where

$$\mathbf{u}_A = \begin{pmatrix} 0 \\ 0 \\ 1 \\ 0 \end{pmatrix}, \quad \mathbf{u}_M = \frac{1}{v} \begin{pmatrix} v_2 \\ -v_1 \\ 0 \\ 0 \end{pmatrix}, \quad (45)$$

and  $\mathbf{u}_\pm$  is the four-element vector satisfying

$$\mathcal{H}_{\text{eff}} \mathbf{u}_\pm = \pm v \mathbf{u}_\pm. \quad (46)$$

As a result, we find an isolated MZM exists at the outer end of the third TS:

$$\gamma_A = \mathbf{u}_A^\dagger \gamma_{\text{eff}} = \gamma_{o,3}, \quad (47)$$

and a MMM splits into the outer edges of the first and second TSs:

$$\begin{aligned} \gamma_M &= \mathbf{u}_M^\dagger \gamma_{\text{eff}} = c_1 \gamma_{o,1} + c_2 \gamma_{o,2}, \\ c_1 &= \frac{v_2}{v}, \quad c_2 = -\frac{v_1}{v}, \end{aligned} \quad (48)$$

which is equivalent to Eq (8) in the main text.

## SCATTERING COEFFICIENTS

In this section, we calculate the scattering coefficients in the presence of the MMM. We start with the scattering matrix at the energy  $E$ , which is given in Eq. (9) of the main text [23–25]:

$$\begin{aligned} S(E) &= \begin{pmatrix} s^{ee} & s^{eh} \\ s^{he} & s^{hh} \end{pmatrix} = 1_6 - 2\pi i W^\dagger [E - \mathcal{H} + i\pi W W^\dagger]^{-1} W, \\ W &= \begin{pmatrix} w & -w \\ 0_{3 \times 3} & 0_{3 \times 3} \end{pmatrix}, \quad w = \begin{pmatrix} w_1 & 0 & 0 \\ 0 & w_2 & 0 \\ 0 & 0 & w_3 \end{pmatrix}, \end{aligned} \quad (49)$$

where the real number of  $w_\alpha$  characterizes the coupling between the electron/hole in the  $\alpha$ -th lead and the MZM at the outer end of the  $\alpha$ -th TS. By using the  $6 \times 6$  unitary matrix in Eq. (29), we can rewrite the scattering matrix as

$$\begin{aligned}
S(E) &= 1_6 - 2\pi i W^\dagger \mathcal{U} [E - \mathcal{U}^\dagger \mathcal{H} \mathcal{U} + i\pi \mathcal{U}^\dagger W W^\dagger \mathcal{U}]^{-1} \mathcal{U}^\dagger W \\
&= 1_6 - 2\pi i W^\dagger [E - \tilde{\mathcal{H}} + i\pi W W^\dagger]^{-1} W \\
&= 1_6 - 2\pi i W^\dagger \begin{pmatrix} E - \mathcal{H}_{\text{eff}} + i\pi \tilde{W} \tilde{W}^\dagger & -\mathcal{V} \\ -\mathcal{V}^\dagger & E - \mathcal{E}_J \end{pmatrix}^{-1} W \\
&= 1_6 - 2\pi i W^\dagger \begin{pmatrix} \tilde{\mathcal{G}}_{\text{mzm}} & \tilde{\mathcal{G}}_{\mathcal{V}} \\ \tilde{\mathcal{G}}_{\mathcal{V}^\dagger} & \tilde{\mathcal{G}}_J \end{pmatrix} W \\
&= 1_6 - 2\pi i \tilde{W}^\dagger \tilde{\mathcal{G}}_{\text{mzm}} \tilde{W},
\end{aligned} \tag{50}$$

where we use  $\mathcal{U}^\dagger W = W$ , and we define,

$$\begin{aligned}
\begin{pmatrix} \tilde{\mathcal{G}}_{\text{mzm}} & \tilde{\mathcal{G}}_{\mathcal{V}} \\ \tilde{\mathcal{G}}_{\mathcal{V}^\dagger} & \tilde{\mathcal{G}}_J \end{pmatrix} &= \begin{pmatrix} E - \mathcal{H}_{\text{eff}} + i\pi \tilde{W} \tilde{W}^\dagger & -\mathcal{V} \\ -\mathcal{V}^\dagger & E - \mathcal{E}_J \end{pmatrix}^{-1}, \\
\tilde{W} &= (\tilde{w}, -\tilde{w}), \quad \tilde{w} = \begin{pmatrix} w \\ 0_{1 \times 3} \end{pmatrix}.
\end{aligned} \tag{51}$$

We specifically obtain

$$\begin{aligned}
\tilde{\mathcal{G}}_{\text{mzm}} &= [E - \mathcal{H}_{\text{eff}} + i\pi \tilde{W} \tilde{W}^\dagger - \mathcal{V}(E - \mathcal{E}_J)^{-1} \mathcal{V}^\dagger]^{-1} = \tilde{\mathcal{G}}_{\text{eff}} [1 - \mathcal{V}(E - \mathcal{E}_J)^{-1} \mathcal{V}^\dagger \tilde{\mathcal{G}}_{\text{eff}}]^{-1}, \\
\tilde{\mathcal{G}}_{\text{eff}} &= [E - \mathcal{H}_{\text{eff}} + i\pi \tilde{W} \tilde{W}^\dagger]^{-1} = [E - \mathcal{H}_{\text{eff}} + i\tilde{\Gamma}]^{-1}, \\
\tilde{\Gamma} &= \text{diag}[\tilde{\Gamma}_1, \tilde{\Gamma}_2, \tilde{\Gamma}_3, 0], \quad \tilde{\Gamma}_\alpha = 2\pi w_\alpha^2.
\end{aligned} \tag{52}$$

Similarly to the discussion in Sec. , in the limit of  $E, E_T, \tilde{\Gamma}_\alpha \ll E_J$ , we can make the replacement of

$$\tilde{\mathcal{G}}_{\text{mzm}} \approx \tilde{\mathcal{G}}_{\text{eff}}, \tag{53}$$

where the contributions from the finite-energy eigenstates at the Josephson junction, described by  $\gamma_{\pm, J}$ , are ignored. Therefore, in the presence of the MMM, the low-energy scattering matrix is evaluated by

$$S(E) = 1_6 - 2\pi i \tilde{W}^\dagger \tilde{\mathcal{G}}_{\text{eff}} \tilde{W} = 1_6 - 2\pi i \tilde{W}^\dagger [E - \mathcal{H}_{\text{eff}} + i\tilde{\Gamma}]^{-1} \tilde{W}. \tag{54}$$

Next, we focus on the scattering matrix in the presence of the MMM of  $\gamma_M$ , which appears at  $v_1, v_2 \neq 0$  and  $v_3 = 0$ . By using the unitary operator of  $\mathcal{U}_{\text{eff}}$ , the scattering matrix is rewritten as

$$\begin{aligned}
S(E) &= 1_6 - 2\pi i \tilde{W}^\dagger \mathcal{U}_{\text{eff}} [E - \mathcal{U}_{\text{eff}}^\dagger \mathcal{H}_{\text{eff}} \mathcal{U}_{\text{eff}} + i\mathcal{U}_{\text{eff}}^\dagger \tilde{\Gamma} \mathcal{U}_{\text{eff}}]^{-1} \mathcal{U}_{\text{eff}}^\dagger \tilde{W} \\
&= 1_6 - 2\pi i W_{\text{eff}}^\dagger [E - \mathcal{E}_{\text{eff}} + i\pi W_{\text{eff}} W_{\text{eff}}^\dagger]^{-1} W_{\text{eff}} \\
&= 1_6 - 2\pi i W_{\text{eff}}^\dagger [E - \mathcal{E}_{\text{eff}} + i\Gamma_{\text{eff}}]^{-1} W_{\text{eff}},
\end{aligned} \tag{55}$$

where

$$\begin{aligned}
W_{\text{eff}} &= \mathcal{U}_{\text{eff}}^\dagger \tilde{W} = \begin{pmatrix} W_0 \\ W_v \end{pmatrix}, \\
W_0 &= (w_0, -w_0), \quad w_0 = \begin{pmatrix} \mathbf{u}_A^\dagger \tilde{w} \\ \mathbf{u}_M^\dagger \tilde{w} \end{pmatrix} = \begin{pmatrix} 0 & 0 & w_3 \\ c_1 w_1 & c_2 w_2 & 0 \end{pmatrix}, \\
W_v &= (w_v, -w_v), \quad w_v = \begin{pmatrix} \mathbf{u}_+^\dagger \tilde{w} \\ \mathbf{u}_-^\dagger \tilde{w} \end{pmatrix}, \\
\Gamma_{\text{eff}} &= \pi W_{\text{eff}} W_{\text{eff}}^\dagger.
\end{aligned} \tag{56}$$

The finite matrix elements in  $\Gamma_{\text{eff}}$  are of the order of  $\Gamma_\alpha$ . Therefore, similarly to the discussion in Sec. , in the limit of  $E, \tilde{\Gamma}_\alpha \ll v$ , we can approximate the scattering matrix as

$$S(E) = 1_6 - 2\pi i W_0^\dagger \left[ E + i\pi W_0 W_0^\dagger \right]^{-1} W_0, \quad (57)$$

where we ignore the contributions from the finite energy states having the energy  $\pm v$ . Eventually, we can rewrite the scattering matrix as

$$S(E) = 1_6 - \begin{pmatrix} A & -A \\ -A & A \end{pmatrix}, \quad (58)$$

$$A = \begin{pmatrix} \frac{i\Gamma_1}{E+i(\Gamma_1+\Gamma_2)} & \frac{i\sqrt{\Gamma_1\Gamma_2}}{E+i(\Gamma_1+\Gamma_2)} & 0 \\ \frac{i\sqrt{\Gamma_1\Gamma_2}}{E+i(\Gamma_1+\Gamma_2)} & \frac{i\Gamma_2}{E+i(\Gamma_1+\Gamma_2)} & 0 \\ 0 & 0 & \frac{i\Gamma_3}{E+i\Gamma_3} \end{pmatrix}, \quad \Gamma_{1(2)} = 2\pi c_{1(2)}^2 w_{1(2)}^2, \quad \Gamma_3 = \tilde{\Gamma}_3 = 2\pi w_3^2,$$

and obtain the scattering coefficients as

$$\begin{aligned} s_{11(22)}^{ee} &= \frac{E + i\Gamma_{2(1)}}{E + i(\Gamma_1 + \Gamma_2)}, \quad s_{11(22)}^{he} = \frac{i\Gamma_{1(2)}}{E + i(\Gamma_1 + \Gamma_2)}, \\ s_{12(21)}^{ee} &= -s_{12(21)}^{he} = \frac{-i\sqrt{\Gamma_1\Gamma_2}}{E + i(\Gamma_1 + \Gamma_2)}, \\ s_{33}^{ee} &= \frac{E}{E + i\Gamma_3}, \quad s_{33}^{he} = \frac{i\Gamma_3}{E + i\Gamma_3}, \\ s_{\alpha 3}^{ee} &= s_{\alpha 3}^{he} = s_{3\alpha}^{ee} = s_{3\alpha}^{he} = 0, \quad (\alpha \neq 3), \end{aligned} \quad (59)$$

which are equivalents to the scattering coefficients in Eq. (12) and Eq. (13) of the main text.

## ADDITIONAL NUMERICAL RESULTS

### The length dependence of the scattering amplitudes

In this section, we show the additional numerical results on the scattering amplitudes calculated for the tight-binding Bogoliubov-de Gennes Hamiltonian used in the main text. The scattering coefficients are computed using the lattice Green's function techniques [54, 55]. In Fig. 3, we show the scattering amplitudes at zero energy as a function of the superconductor length  $L$ , where we only show  $|s_{12}^{he}|^2$  in the main text. The parameters are chosen to be the same as those in Fig. 2(a) of the main text. We clearly find the plateau satisfying

$$|s_{\alpha\beta}^{ee}|^2 = |s_{\alpha\beta}^{he}|^2 = 1/4, \quad (\alpha, \beta = 1, 2) \quad (60)$$

in the broad range of  $L$ , which agrees with the analytical results in Eq. (59) at  $\Gamma_1 = \Gamma_2$ . Therefore, as also discussed in the main text, we numerically demonstrate the nonlocal resonant scatterings of the MMM within the tight-binding model.

### Zero-frequency noise power

In this section, we show the additional numerical results on the zero-frequency noise power calculated for the tight-binding Bogoliubov-de Gennes Hamiltonian used in the main text. We evaluate the zero-frequency noise power at zero temperature by [33, 34]

$$\begin{aligned} P_{\alpha\beta} &= \frac{e^2}{h} \int_0^{eV} \mathcal{P}_{\alpha\beta}(E) dE, \\ \mathcal{P}_{\alpha\beta}(E) &= \delta_{\alpha\beta} \sum_{\eta=e,h} p_{\alpha\alpha}^{\eta\eta} - \sum_{\eta,\zeta} \sigma_\eta \sigma_\zeta p_{\alpha\beta}^{\eta\zeta} p_{\beta\alpha}^{\zeta\eta}, \quad p_\alpha^{\eta\zeta} = \sum_{\gamma=1,2,3} s_{\alpha\gamma}^{\eta e} (s_{\beta\gamma}^{\zeta e})^*, \end{aligned} \quad (61)$$

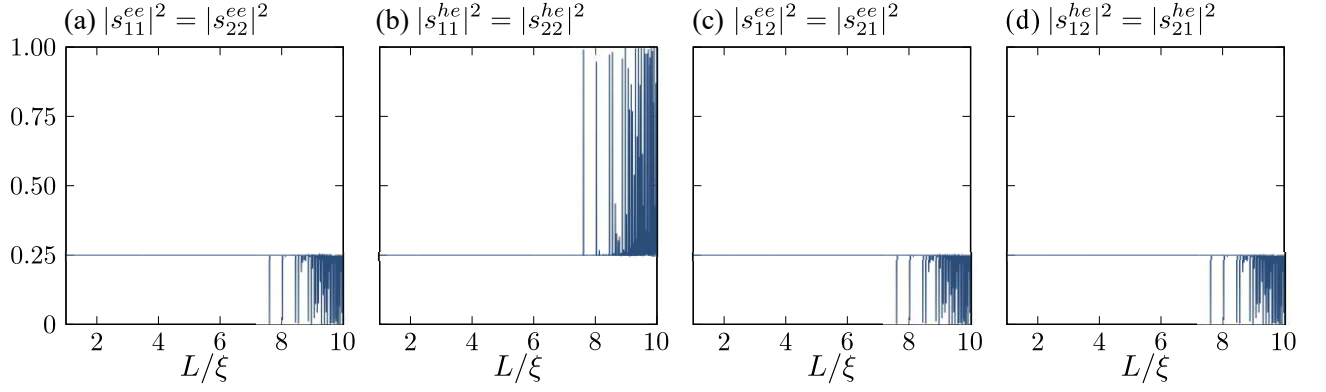


FIG. 3. Scattering amplitudes at zero energy as a function of the superconductor length. We show (a)  $|s_{11}^{ee}(E=0)|^2 = |s_{22}^{ee}(E=0)|^2$ , (b)  $|s_{11}^{he}(E=0)|^2 = |s_{22}^{he}(E=0)|^2$ , (c)  $|s_{12}^{ee}(E=0)|^2 = |s_{21}^{ee}(E=0)|^2$ , and (d)  $|s_{12}^{he}(E=0)|^2 = |s_{21}^{he}(E=0)|^2$ .

where  $\sigma_\eta = 1$  ( $-1$ ) for  $\eta = e$  ( $h$ ), which is equivalent to Eq. (18) of the main text. In Fig. 4, we show the zero-frequency noise power  $P_{\alpha\beta}$  for  $\alpha, \beta = 1, 2$  as a function of the bias voltage. Specifically, we plot

$$F_{\alpha\beta}(eV) = \frac{P_{\alpha\beta}(eV)}{I_1(eV) + I_2(eV)}, \quad (62)$$

where  $I_\alpha(eV)$  is the time-averaged current in the  $\alpha$ -th lead wire. The parameters are chosen to be the same as those in Fig. 2(c) of the main text. At the zero-bias voltage limit, we clearly find the relations,

$$2|P_{12}| = P_{11} + P_{22}, \quad P_{11} + P_{22} + P_{12} + P_{21} = 0, \quad (63)$$

which agree with Eq. (20) and Eq. (21) in the main text, respectively. Therefore, we confirm the anomalies in the zero-frequency noise power due to the nonlocally entangled resonant scatterings of the MMM on the tight-binding model.

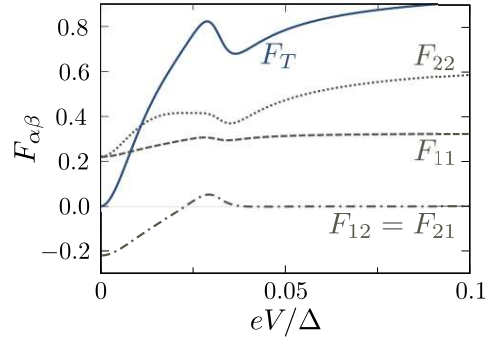


FIG. 4. Zero-frequency noise power normalized by the charge current as a function of the bias voltage. The solid line represents  $F_T = F_{11} + F_{22} + F_{12} + F_{21}$ .